Jurnal Kejuruteraan 34(6) 2022: 1077-1083
https://doi.org/10.17576/jkukm-2022-34(6)-08

Effect of Oxide Flux Particle Size on Weld Bead Morphology of Hastelloy C-22

Dixit Patel[a,b*] , Suketu Jani[c] & Darshit Shah[d]

[a]*Mechanical Engineering Department, Indus University, India*
[b]*Mechanical Engineering Department, GEC-Gandhinagar, India*
[c]*Automobile Engineering Department, Indus University, India*
[d]*Mechanical Engineering Department, L.D. College of Engineering, India*

**Corresponding author: dixitpatel.rs@indusuni.ac.in*

Received 10 January 2022, Received in revised form 28 February 2022
Accepted 29 March 2022, Available online 30 November 2022

ABSTRACT

Activated tungsten inert gas welding (ATIG) welding is a new approach to Tungsten Inert Gas (TIG) welding that has the potential to improve weld penetration. This paper investigates the effect of micro and nanoparticle size oxide flux during TIG welding of Hastelloy C-22. The effect of SiO_2 and Al_2O_3 oxide fluxes in terms of particle size and thermal stability on surface appearance, bead geometry, and microhardness of the fusion zone of hastelloy C-22 is investigated. The surface appearance of ATIG weld has a better appearance using nanoparticle size oxide flux when compared with the same micro size oxide flux. A slag layer produced by nano flux decomposition during TIG welding is very less compared to micro oxide fluxes. Nanoparticle SiO_2 flux has the potential to improve weld penetration and depth to width (D/W) ratio in the generated weldment when compared to microparticle SiO_2 flux during TIG welding Process. When nanoparticle Al_2O_3 is used in TIG welding, weld penetration or the D/W ratio do not increase significantly. Due to the high voltage produced at the same arc length, TIG welding with nanoparticle SiO_2 flux produces a high heat input. Furthermore, higher arc temperatures produce by nanoparticle fluxes at the arc column, resulting in increased penetration depth.

Keywords: ATIG; Flux; Slag; Penetration depth; weld bead width

INTRODUCTION

Tungsten Inert Gas (TIG) welding is one of the most commonly used welding processes due to its aesthetic look and well-controlled process parameter to get desired bead properties of different metals and alloys but the only disadvantage during the process is its shallow penetration and due to this number of pass required to full penetration is more compare to other arc welding process (Nanavati et al. 2021). Many studies and alternatives have been developed to improve the productivity and depth of penetration during the TIG welding process. Activated TIG is the best option for increasing productivity among these developments (Rana et al. 2021).

The Paton institute of welding coined novel energy efficient variant of TIG welding known as Activated tungsten Inert Gas (ATIG) welding to enhanced depth of penetration (Vora et al. 2019). In this process, activated flux like oxides, halides, or sulfides is mixed with a solvent like acetone or methanol to prepare penetration enhancing paint as shown in Figure 1. During the welding process these activated fluxes are melted and increased depth of penetration (Deep et al. 2021).

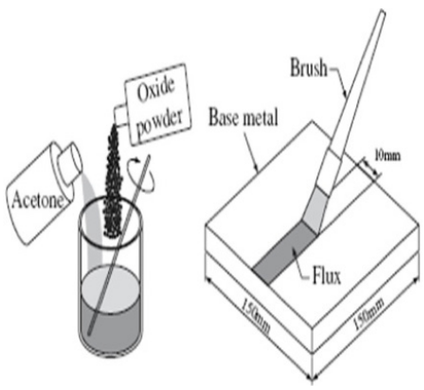

FIGURE 1. schematic diagram of production of PEP paste

The mechanisms responsible for improving weld penetration are mainly reverse marangoni and arc constriction(Manikandan et al. 2018). During the welding process, a large amount of heat is generated in the arc column's center and is reduced at its periphery (Jaypuria et al. 2019). Figure 2(a) shows that at the center of the weld, lower surface tension and higher temperature prevail, while

at the edge, higher surface tension and lower temperature prevail. As a result, molten metal flows from the lower surface tension to the higher surface tension outward side, resulting in shallow penetration during normal TIG welding (Mills et al. 1998). In ATIG welding activated flux is applied on the surface before the TIG welding process. And These molten fluxes influence the weld metal chemistry and change the surface tension gradient from negative to positive as shown in Figure 2(b) and due to this molten metal flow from edge to center and produced a high depth of penetration (Patel et al. 2019). This mechanism is known as the reverse marangoni effect.

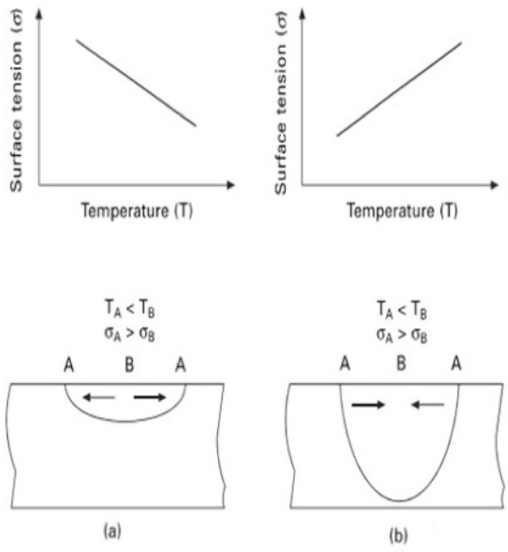

FIGURE 2. Effect of surface tension on molten metal flow during (a) TIG (b) ATIG process

Arc constriction is the other mechanism. Because flux acts as an insulator during ATIG welding, the current density at the center of the arc column increases, higher magnetic forces are generated, and the depth of penetration is increased (Jayakrishnan et al. 2017). Also, flux acts as an anode spot, attracting electrons, which impinge at the surface at a high velocity, improving weld penetration(Mills and Keene, 1990).

Tseng et al. (Tseng, 2013)performed ATIG welding on ASS steel using 2.4 mm and 3.2 mm tungsten electrodes and discovered that the smaller diameter tip of the tungsten electrode melted during ATIG welding, while the 3.2 mm diameter electrode showed no wear. Hung et al (Huang et al. 2005) study the effect of different oxides fluxes on austenitic stainless steel and found that arc voltage significantly increased during the use of activated fluxes than normal TIG welding. In addition, using MnO_2 and ZnO fluxes, full penetration of 6mm thickness was achieved in a single pass ATIG welding. Increasing the arc voltage increased the delta ferrite content in the weld zone, lowering the susceptibility to hot cracking (Sawickij et al. 2001) . During the ATIG process, Morisada et al. discovered that the plasma arc column and anode spot play important roles in producing narrow beads and deeper penetration (Morisada et al. 2014). Vasudevan (Vasudevan, 2017)developed a flux for 304L and 316L to improve up to 12 mm during the ATIG process. Increased weld penetration is caused by the arc constriction and reverse marangoni effect, and the weld zone's grain will be finer, resulting in increased transverse strength and impact value. SiO_2 flux increases arc voltage more than TiO_2 flux, according to Li et al. (Li et al. 2007). SiO_2 flux also has a higher arc deflection. The addition of nitrogen to argon improves penetration depth during ATIG welding(Huang, 2009). Tseng et al (Tseng and Lin, 2014)also study the effect of micro and nanoparticles flux on UNS S31603 stainless steel and found nano flux gives a higher D/W ratio and narrow HAZ compared to micro-sized flux. Xie et al (Xie et al. 2015)study the effect of nanoparticles during TIG welding of magnesium alloy and found increasing the surface coating thickness, degrading the macro appearance of the weld bead also the microhardness of HAZ will reduce with increasing the coating thickness.

Ni-base alloys are widely used in industries from cryogenic to high temperature applications due to excellent corrosion resistance under critical environments (Arulmurugan et al. 2019) (Saunders et al. 2004)work on the development of thermodynamic modelling tools for application to multi-component Ni-based superalloys has been presented. Such modelling has become quite widespread, providing significant benefit. However, its applicability often falls short from directly providing the information that is actually required and, by itself, cannot be directly used to model properties being targeted by the end user, e.g. TTT/CCT diagrams, mechanical properties, thermophysical and physical properties. To overcome these limitations a new computer programme has been developed, called JMatPro, an acronym for Java-based Materials Properties software. The properties which can be calculated are wide ranging, including thermo-physical and physical properties (from room temperature to the liquid state . Hastelloy C-22 is the most corrosive-resistant nickel-based alloy, and it can be welded using the TIG welding process (Wang et al. 2014) (Dhananchezian and Rajkumar 2020). In this study, different oxide fluxes were used during TIG welding to increase the weld penetration (D) and the D/W ratio of the weldment. The effect of nano and micro size activated fluxes on the weld bead surface, slag detachability, and weld geometry is also investigated in this study.

MATERIALS AND METHODS

Hastelloy C-22 alloy plate of 6 mm thickness was used in this study and the chemical composition of it is shown in Table 1. All plates were rough ground to remove oxides from the surface and cleaned with acetone before welding.

TABLE1. Chemical Composition in % of the weight of Hastelloy C-22

Ni	Mo	Cr	Fe	W	Co	Mn	C
Balance	13.3	20.6	5	2.7	1.2	0.21	0.002

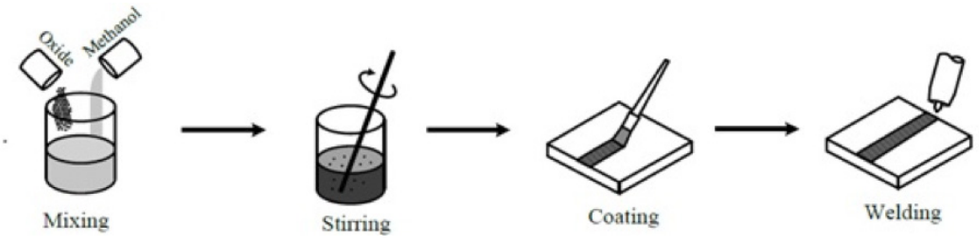

FIGURE 3. Procedure for making penetrating enhancing paint (PEP)

TABLE 2. Physical properties of micro and nano particles of oxide flux

	SiO_2		Al_2O_3	
	Micro particle	Nano particle	Micro particle	Nano particle
Particle size	<5 µm	30-50 nm	<5 µm	30-50 nm
Density (gm/cm^2)	2.35	2.15	3.95	3.84

The oxide fluxes SiO_2 and Al_2O_3 of micro and nano size were used in this study, and their physical properties and appearance are listed in Table 2. This oxides flux is mixed with acetone with appropriate percentage and stirred until it makes pint like consistency as shown in Figure 3 to make penetration enhancing paste (PEP). This PEP paste was applied on the alloy C-22 plate using a paintbrush of 12 mm width. After applying the paste on the surface sufficient time is given to evaporate acetone and adhered flux layer on the plate surface.

The welding was performed using direct current electrode negative polarity with a 3.2 mm diameter, 2% thoriated tungsten electrode (EWTH-2). The experiments are conducted by connected TIG welding torch on a motorized trolley as shown in Figure 4. All bead on plate single pass autogenous TIG and ATIG welding was done on a mechanized system with a constant current power supply and different nano and micro size oxide fluxes. All of the experiments are carried out under the same conditions and parameters as described in Table 3. A change in the variation in the voltage during the weld bead is observed. Also, at a 10 mm distance from the center K type thermocouple sensor was placed to measure the temperature of the fusion zone. Weld bead surface appearance and slag detachability are visually inspected and analyzed.

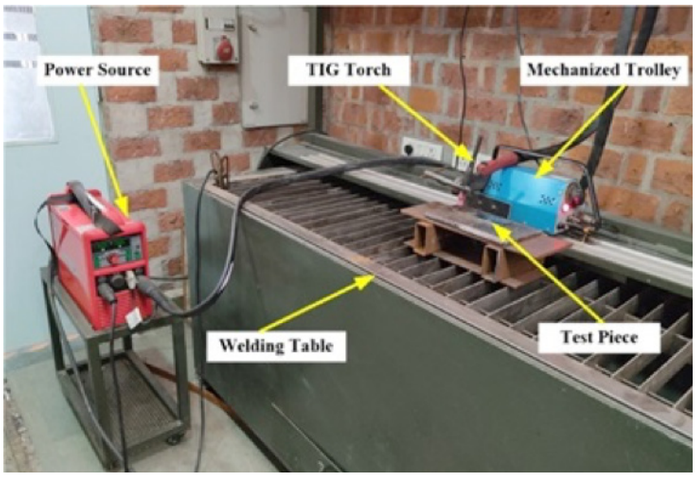

FIGURE 4. Experimental setup of ATIG welding

All weld beads are cut perpendicular to the direction of the weld, and macro samples are extracted. This sample is rough ground, then fine polished 100X, 200X, 400X on SiC grit paper, and finally polished with diamond. Each sample was etched with 50V passing through electrolyte solution of 1:10 ratio of oxalic acid and 100 ml water. On an Olympus 10X macroscope, the weld penetration and weld bead width are measured. Additionally, Vickers microhardness measurements Normal TIG and ATIG with nano and microparticle oxide fluxes at the fusion zone using microhardness tester (Make: OMNITECH, Model: S Auto I).

TABLE 3. Welding parameters and fluxes used for TIG and ATIG process

W electrode tip angle	60 degree
Torch angle	90 degree
Arc Current	200 amp
Arc length	3mm
Welding speed	170 mm/min
Shielding gas	Ar
Gas flow rate	15 lpm

RESULT AND DISCUSSION

WELD BEAD APPEARANCE

Weld bead of TIG welding gives aesthetic look compared to all other conventional welding processes. This is due to no slag or spatters produced during the TIG welding process as shown in Figure 5(a). While ATIG welding produced excessive slag and rough surface compared to normal TIG welding. During ATIG welding flux melted during the welding process and form a slag that is less dense than the molten surface so it will float over the molten metal and generate a slag layer after solidification. The particle size of flux affects the slag layer produced during ATIG welding. Nanosize SiO_2 flux (as shown in Figure 5(d)) produced very little slag produced compared to microparticle SiO_2 (shown in Figure 5(b)). A similar result was also found when we compare micro and nano size Al_2O_3 weld bead surface as shown in Figure 5 (c) & (e). Also, weld surface produced using nanoparticle flux gives a better surface appearance than the micro size of flux.

During welding, nanoparticle SiO_2 flux is completely melted, whereas nanoparticle Al_2O_3 has some unmelted flux visible on each side of the weld bead. This is because the melting point of Al_2O_3 is higher than that of SiO_2. The melting point of flux deviates from its bulk materials and becomes a size dependent property as the particle size of flux decreases below a critical value. The melting point of nanoparticle fluxes is lower than that of microparticle fluxes due to the higher surface to volume ratio (Antoniammal and Arivuoli 2012). As a result, the welding arc heat may have melted the nanoparticle oxides more easily. A TIG weld made with nanoparticle oxide has less flux slag on the surface than a TIG weld made with the same type of microparticle oxide.

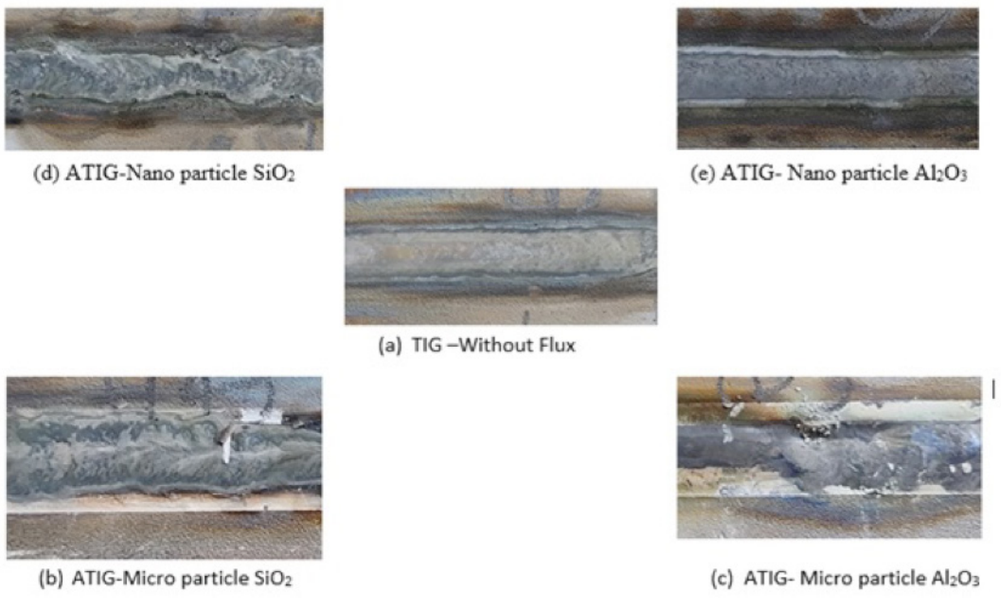

FIGURE 5. weld bead surface appearance of TIG and ATIG weld joint

WELD BEAD GEOMETRY

Activated flux during the TIG welding process creates an effect on molten metal flow and arc characteristics and enhances the depth of penetration dramatically. The major responsible mechanism for weld penetration enhancement is reverse marangoni and arc constriction. The weld bead dimension in terms of depth of penetration (D), weld bead width (W), and depth to width ratio (D/W) of TIG, ATIG using micro and nanoparticle fluxes presented in Table 4. and its macrograph has shown in Figure 6. In ATIG welding with nano and micro size oxide fluxes Depth of penetration increased and weld bead width decreased. The mechanisms are responsible for this phenomenon listed in Table 4.

TABLE4. effect of flux particle size on weld bead profile

Sr. No	Process	Flux	Particle Size	D (mm)	W (mm)	D/W	Peak Temp (°C)	Voltage	Reverse marangoni	Arc constriction
1	TIG	-	-	1.81	10.30	0.18	612	15.2	Absent	Absent
2	ATIG	SiO_2	Micro	3.10	9.13	0.34	756	16.6	Present	Present
3		SiO_2	Nano	4.06	7.75	0.52	805	17	Present	Present
4		Al_2O_3	Micro	2.41	10.28	0.23	680	16.4	Present	Absent
5		Al_2O_3	Nano	3.17	9.38	0.34	690	16.4	Present	Absent

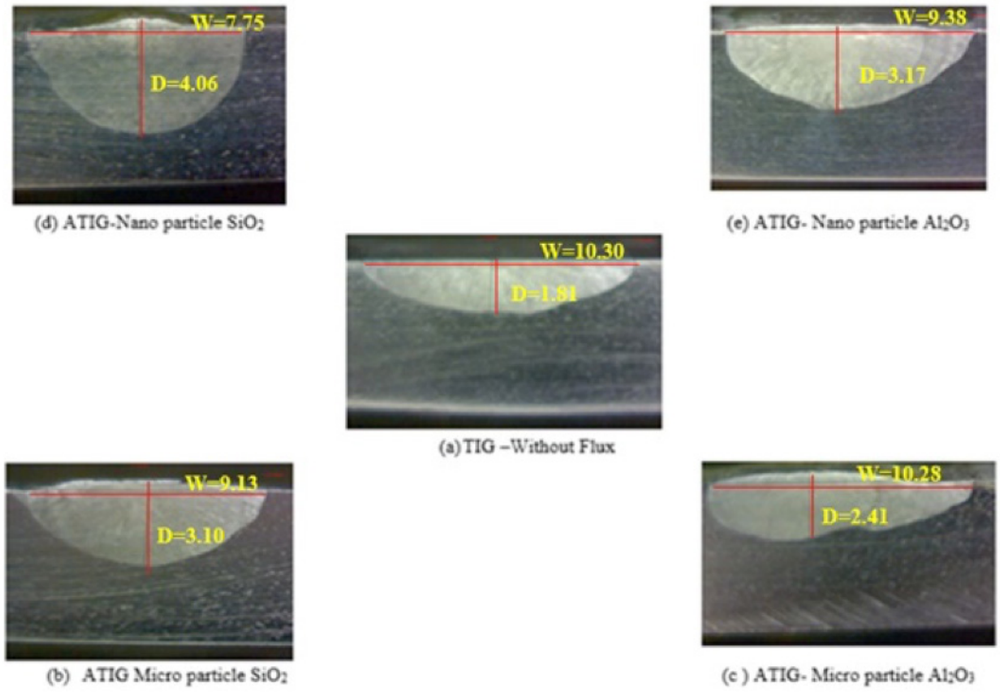

FIGURE 6. Macro graph of weld bead geometry

All the experiments are carried out with the same welding parameters but the use of activated flux increased arc voltage 1-2 V for the same arc length compared to normal TIG welding. The arc voltage is directly proportional to heat input, as arc voltage increased amount of heat generated during the welding increased and its leads to an increase in penetration. The peak temperature at 10 mm distance from the weld centerline is measured and the highest depth of penetration found ATIG welding using nano size SiO_2 oxide flux and both arc constriction and reverse marangoni effect observed. Higher the temp shows the high amount of heat intensity generated at the center and it will have reduced from center to outside of the arc. High temp leads to arc constriction effect during the welding. Nanoparticle oxide fluxes are easier to melt and vaporize than microparticle oxide fluxes. The vaporized flux constricts the arc plasma by capturing electrons from the arc column's outer regions and transporting them to the center. The decomposition of oxide flux will produce dissociated ions, which will affect electron absorption and result in the formation of negative charge particles. As a result, current flow to the central region of the arc column increases, as does the arc plasma's current density, and the arc temperature at the molten pool surface rises Furthermore because nano-sized oxide particles have

greater electrical conductivity than micro-sized particles, their current resistivity is higher, resulting in greater arc constriction (Minea, 2019) (Yuliza et al. 2015). In comparison to Al_2O_3, SiO_2 flux has a greater depth of penetration and a narrower weld bead width for micro and nanoparticle size. A similar result was obtained when the nano and microparticle fluxes of the same component were compared. Figure 7 shows that ATIG welding with nanoparticles SiO_2 flux gives the highest depth of penetration, D/W ratio, and lowest weld bed width.

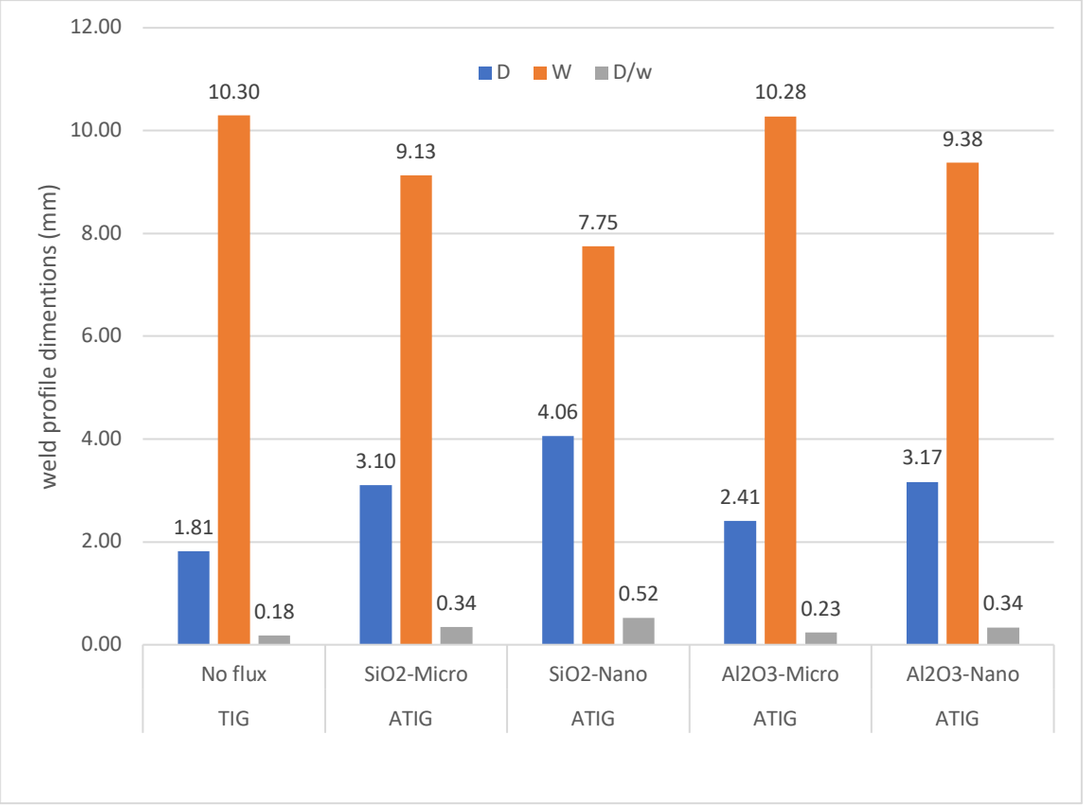

FIGURE 7. Weld bead geometry comparison for TIG and ATIG- micro/nano oxides fluxes

WELD BEAD APPEARANCE

Vickers Micro-hardness measurements were carried out at 1kg load for 10 sec dwell time on a transverse cross-section specimen of fusion zone. The average hardness of the base metal is 255 Hv. The increase in hardness of the weld zone was observed for both TIG welding and ATIG Welding compared to a base metal. Weld zone of TIG welding has microhardness of 267 Hv. The weld zone generated from ATIG welding of nanoparticle SiO_2 (278 Hv) has a higher hardness value than micro particle SiO_2 (273 Hv). Likewise, the weld zone of ATIG welding using micro particles and nanoparticle Al_2O_3 have hardness values of (268 Hv) and 271 Hv respectively. The weld zone produced using nanoparticle flux ATIG welding has a higher hardness value than micro particle flux ATIG welding due to higher arc voltage and peak temperature generated during nanoparticle ATIG welding.

CONCLUSIONS

The following conclusions can be drawn from the results presented in this work:

1. In comparison to TIG welding, the use of oxides flux increased the depth of penetration and the D/W ratio.
2. When ATIG welding with nano-sized oxide fluxes, the fluxes completely melt and produce slag, while with micro-sized fluxes, a small amount of un-melted flux residue remains after welding.
3. The ripples in ATIG welding with nanoparticle flux are more even than with micro size flux.
4. ATIG welding with a micro size oxide flux produces a larger slag than ATIG welding with a nano size oxide flux. It's also more difficult to clean up than nanoparticle flux slag.
5. ATIG welding with SiO_2 and Al_2O_3 yields higher DOP and D/w rations when nanoparticles flux is used instead of microparticle flux. Nano size SiO_2 flux, on the other hand, produced the highest DOP and D/W ratio than nano size Al_2O_3 flux.

6. ATIG welding using nanoparticle flux produced higher hardness in the weld zone than micro particle flux.

ACKNOWLEDGEMENT

The authors would like to thank Indus University, India for their support.

DECLARATION OF COMPETING INTEREST

None

REFERENCES

Antoniammal, P. & Arivuoli, D., 2012. Size and shape dependence on melting temperature of gallium nitride nanoparticles. *J. Nanomater* 415797. https://doi.org/10.1155/2012/415797

Arulmurugan, B., Modi, K., Sanjay, A.P., Yashwant, P.A., Rickwith, N., Mohan, C.G., Subramani, P., Agilan, M., Manikandan, M. & Arivazhagan, N. 2019. Effect of post-weld heat treatment on the microstructure and tensile properties of electron-beam-welded 21st century nickel-based super alloy 686. *Sādhanā* 44: 38. https://doi.org/10.1007/s12046-018-1047-z

Deep, A., Singh, V., Ashutosh, S., Chandrasekaran, M. & Patel, D. 2021. Performance of weld bead profile during A-TIG welding on nitrogen alloyed stainless steel. *Eng. Res. Express*. https://doi.org/10.1088/2631-8695/ac3770

Dhananchezian, M. & Rajkumar, K. 2020. Cryogenic turning of Hastelloy C-22. *Mater. Today Proc.* 22: 3075–3081. https://doi.org/10.1016/j.matpr.2020.03.443

Huang, H.-Y., 2009. Effects of shielding gas composition and activating flux on GTAW weldments. *Mater. Des.* 30: 2404–2409. https://doi.org/10.1016/j.matdes.2008.10.024

Huang, H.Y., Shyu, S.W., Tseng, K.H. & Chou, C.P. 2005. Evaluation of TIG flux welding on the characteristics of stainless steel. *Sci. Technol. Weld. Join.* 10: 566–573. https://doi.org/10.1179/174329305X48329

Jayakrishnan, S., Chakravarthy, P. & Muhammed Rijas, A., 2017. Effect of flux gap and particle size on the depth of penetration in FBTIG welding of aluminium. *Trans. Indian Inst. Met.* 70: 1329–1335. https://doi.org/10.1007/s12666-016-0929-1

Jaypuria, S., Khandai, S., Ranjan Mahapatra, T. & Singh, A. 2019. Development of activated flux for deep penetration in GTAW. *Mater. Today Proc.* 18: 4703–4710. https://doi.org/10.1016/j.matpr.2019.07.456

Li, Q., Wang, X., Zou, Z. & Wu, J. 2007. Effect of activating flux on arc shape and arc voltage in tungsten inert gas welding. *Trans. Nonferrous Met. Soc. China* 17: 486–490. https://doi.org/10.1016/S1003-6326(07)60120-4

Manikandan, M., Raj, A.D., Kumar, M.S., Arivazhagan, N., Gunachandran, R., Kumar, J.K.M., Vignesh, V. & Yoganathan, D. 2018. Investigation on microstructure, micro segregation and mechanical properties of ATIG welded alloy C-276. *Mater. Today Proc.* 5: 6702–6710. https://doi.org/10.1016/j.matpr.2017.11.327

Mills, K.C. & Keene, B. J. 1990. Factors affecting variable weld penetration. *Int. Mater. Rev.* 35: 185–216. https://doi.org/10.1179/095066090790323966

Mills, K.C., Keene, B.J., Brooks, R.F. & Shirali, A. 1998. Marangoni Effects in Welding. *Philos. Trans. Math. Phys. Eng. Sci.* 356: 911–925.

Minea, A.A., 2019. A review on electrical conductivity of nanoparticle-enhanced fluids. *Nanomaterials* 9: 1592. https://doi.org/10.3390/nano9111592

Morisada, Y., Fujii, H. & Xukun, N., 2014. Development of simplified active flux tungsten inert gas welding for deep penetration. *Mater. Des.* 1980-2015 54: 526–530. https://doi.org/10.1016/j.matdes.2013.08.081

Nanavati, P.K., Badheka, V.J., Idhariya, J. & Solanki, D. 2021. Comparisons of different oxide fluxes in activated gas tungsten arc welding of duplex stainless steels for improved depth of penetration and pitting corrosion resistance. *Adv. Mater. Process. Technol.* 1–18. https://doi.org/10.1080/2374068X.2021.1916283

Patel, N. P., Badheka, V. J., Vora, J. J. & Upadhyay, G. H. 2019. Effect of Oxide Fluxes in Activated TIG Welding of Stainless Steel 316LN to Low Activation Ferritic/Martensitic Steel (LAFM) Dissimilar Combination. *Trans. Indian Inst. Met.* 72: 2753–2761. https://doi.org/10.1007/s12666-019-01752-7

Rana, H., Badheka, V., Patel, P., Patel, V., Li, W. & Andersson, J. 2021. Augmentation of weld penetration by flux assisted TIG welding and its distinct variants for oxygen free copper. *J. Mater. Res. Technol.* 10: 138–151. https://doi.org/10.1016/j.jmrt.2020.12.009

Saunders, N., Guo, Z., Li, X., Miodownik, A.P. & Schille, J.-Ph. 2004. Modelling the Material Properties and Behaviour of Ni-Based Superalloys, in: Superalloys 2004 (Tenth International Symposium). Presented at the Superalloys, TMS, pp. 849–858. https://doi.org/10.7449/2004/Superalloys_2004_849_858

Sawickij, M.M., Mielniczuk, G.M., Lupan, A.F., Sawickij, A.M., Olejnik, O.I., 2001. Activating fluxes in inert gas-shield welding of steels. *Weld. Int.* 15: 677–683. https://doi.org/10.1080/09507110109549424

Tseng, K.-H. 2013. Development and application of oxide-based flux powder for tungsten inert gas welding of austenitic stainless steels. *Powder Technol.* 233: 72–79. https://doi.org/10.1016/j.powtec.2012.08.038

Tseng, K.-H. & Lin, P.-Y. 2014. UNS S31603 stainless steel tungsten inert gas welds made with microparticle and nanoparticle oxides. *Materials* 7: 4755–4772. https://doi.org/10.3390/ma7064755

Vasudevan, M., 2017. Effect of A-TIG Welding Process on the Weld Attributes of Type 304LN and 316LN Stainless Steels. *J. Mater. Eng. Perform.* 26: 1325–1336. https://doi.org/10.1007/s11665-017-2517-x

Vora, J.J., Abhishek, K. & Srinivasan, S. 2019. Attaining optimized A-TIG welding parameters for carbon steels by advanced parameter-less optimization techniques: with experimental validation. *J. Braz. Soc. Mech. Sci. Eng.* 41: 261. https://doi.org/10.1007/s40430-019-1765-0

Wang, Q., Bai, S. & Liu, Z. 2014. Corrosion behavior of Hastelloy C22 coating produced by laser cladding in static and cavitation acid solution. *Trans. Nonferrous Met. Soc. China* 24: 1610–1618. https://doi.org/10.1016/S1003-6326(14)63232-5

Xie, X., Shen, J., Cheng, L., Li, Y. & Pu, Y. 2015. Effects of nano-particles strengthening activating flux on the microstructures and mechanical properties of TIG welded AZ31 magnesium alloy joints. *Mater. Des.* 81: 31–38. https://doi.org/10.1016/j.matdes.2015.05.024

Yuliza, E., Murniati, R., Rajak, A., Khairurrijal & Abdullah, M. 2015. Effect of particle size on the electrical conductivity of metallic particles. Presented at the 2014 International Conference on Advances in Education Technology (ICAET-14), Bandung, Indonesia. https://doi.org/10.2991/icaet-14.2014.37